

Effects of Electron Transfer in Model Catalysts Composed of Pt Nanoparticles on CeO₂(111) Surface

Sergey M. Kozlov,^{a,*} Konstantin M. Neyman^{a,b,*}

^a *Departament de Ciència de Materials i Química Física and Institut de Química Teòrica i Computacional, Universitat de Barcelona, c/ Martí i Franquès 1, 08028 Barcelona, Spain*

^b *ICREA (Institució Catalana de Recerca i Estudis Avançats), Pg. Lluís Companys 23, 08010 Barcelona, Spain*

Highlights:

- ~1.5 nm particles forming Pt₁₂₂{111}||CeO₂(111) and Pt₉₅{100}||CeO₂(111) interfaces
- Simulation approach enabling full control of electron transfer in model catalysts
- Interaction of Pt particles with CeO₂(111) shifts d-states of Pt to lower energies
- Pt-ceria interaction increases average Pt-Pt distances in the supported particles
- Geometry and DOS of the Pt particles are slightly altered by the electron transfer

Abstract. Interactions between transition metal nanoparticles and reducible oxide supports are thought to significantly affect the performance of many catalysts. Usually, several metal-support effects act together and cannot be separated from each other. Herein, by means of density-functional calculations we succeeded to single-out and quantify effects of the metal-support electron transfer on the structure and electronic properties of important model Pt-ceria catalysts. Namely, we considered ~1.5 nm large Pt₉₅ and Pt₁₂₂ particles supported on CeO₂(111). We show that Pt-ceria interactions notably reconstruct Pt nanofacets forming the interface and shift valence d-states of the Pt particles. These effects are rather insensitive to the Pt-ceria electron transfer, at variance with the electronic structure of oxygen anions at the interface, which is significantly affected by the electron transfer. The findings of this work and the special modelling approach applied pave the way for deeper analysis of electronic metal-support interactions in catalysis.

Keywords: DFT, Pt, ceria, electronic metal-support interaction, electron transfer, electronic structure

* Corresponding authors. *E-mail addresses:*

sergey.kozlov@kaust.edu.sa (S.M. Kozlov), konstantin.neyman@icrea.cat (K.M. Neyman)

[†] Present address: KAUST Catalysis Research Center, Physical Sciences and Engineering Division, King Abdullah University of Science and Technology, Thuwal 23955-6900, Kingdom of Saudi Arabia

1 **1. Introduction**

2 Transition metal nanoparticles (NPs) supported on oxides are the foundation of many
3 indispensable catalysts, such as (de-)hydrogenation catalysts [1,2], catalysts for treatment of
4 exhaust gases [3,4] and for environmentally friendly energy technologies [5,6]. Performance
5 of such catalysts depends equally strongly on the active material and its support, their nature
6 and their structure [7,8]. Presently, there is an increasing understanding of how the catalytic
7 activity is shaped by low-coordinated atoms on metal NPs [9,10], the modification of the
8 latter by the reaction environment [11,12] and the chemical ordering in alloy NPs [13,14]. The
9 effects of nanostructuring of the oxide support on the catalyst properties have also been
10 investigated [15,16]. Yet, relatively little is known regarding atomic and electronic
11 mechanism of electronic metal-support interactions [17–19]. In particular, it is largely
12 unexplored how metal-support electron transfer may affect the catalyst [20,21]. Partially, this
13 is because the magnitude of the electron transfer is hard to measure and control both in
14 experiments and simulations.

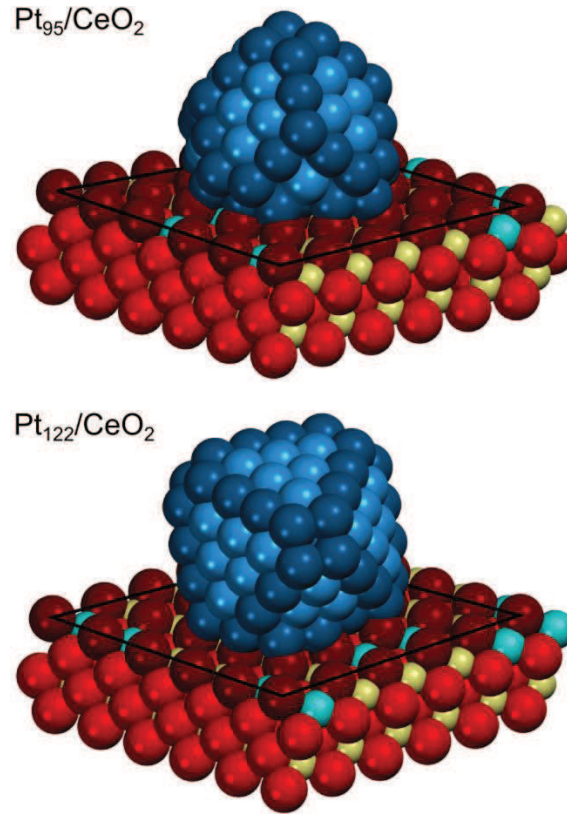
15 Fortunately, it is possible to quite accurately measure the electron transfer for one of the
16 technologically important oxide supports, CeO_x [3,22,23]. The ability of cerium oxide
17 supports to increase the activity of catalysts [15,24] is often related to their reducibility
18 [22,25,26], i.e. the ease of reduction of particular Ce^{4+} cations to localized Ce^{3+} [27,28] and
19 the related ability to easily store/release lattice O [29,30]. These virtues also allow one to
20 measure the charge transferred to cerium oxide by counting Ce^{3+} cations with a highly
21 sensitive technique called resonant photoemission spectroscopy [31,32]. In turn, in electronic
22 structure simulations Ce^{3+} cations are easily distinguished from Ce^{4+} ones by their well-
23 defined magnetic moment. From the amount of Ce^{3+} cations in the system one can
24 unequivocally quantify the magnitude of metal-support electron transfer both in experiments
25 [23,33] and simulations [26]. Moreover, in simulations one could also tune the number of
26 transferred electrons from the metal to the oxide by enforcing a particular magnetization (and,
27 hence, the charge) on every Ce cation in the system [23,34]. This allows one to study the
28 electronic metal-oxide interaction as a function of the amount of the electron transfer.

29 Herein, we have studied the electron transfer and the electronic metal-support interaction
30 in a particularly important catalytic system, Pt nanoparticles deposited on ceria [35–38].
31 Although Pt-ceria interaction is very complex and may include hydrogen spillover [25,39] and
32 reverse oxygen spillover [34,40], besides the electron transfer [23,41], we deliberately focus
33 on the latter. In particular, we have considered the electron transfer from Pt nanoparticles to

1 the idealized CeO₂(111) support without O vacancies, because the presence of the latter was
2 shown to decrease the number of transferred electrons [23]. Note that an even higher
3 magnitude of the electron transfer may be expected between Pt nanoparticles and the
4 nanostructured ceria support due to the increased reducibility of the latter [26,30].

5 In the following, we investigate ceria-supported Pt NPs of ~100 atoms and ~1.5 nm in
6 size, which is qualitatively larger than those in previous computational investigations [17,42]
7 and approaches common NP sizes in applications of Pt [43,44]. In fact, metal NPs of this size
8 usually belong to the scalable with size regime, so their properties can be extrapolated to
9 those of larger particles [45,46]. To the best of our knowledge, the shape of Pt nanoparticles
10 on the CeO₂(111) support and the structure of the formed metal-oxide interface are yet to be
11 characterized with the sufficiently high resolution that would allow one to design
12 computational models based on the experimental results [47]. Despite of some understanding
13 of the interface structure between the extended Pt(111) and CeO₂(111) surfaces from the
14 experimental [48,49] and computational [50,51] points of view, it is not possible to apply this
15 knowledge to precisely design the interface between the considered Pt NPs and the ceria
16 support. In the absence of sufficiently accurate atomic structures of Pt NPs on CeO₂(111)
17 derived from observations, models of ceria-supported Pt nanoparticles in the present work
18 were designed following the shapes of Pt NPs supported on MgO(100) [52–54]. The
19 considered nanoparticles featured fully relaxed *fcc* structure and a shape in line with the
20 Wulff-Kaishev construction. The present work focuses on the investigation of Pt₉₅ and Pt₁₂₂
21 nanoparticles forming Pt{100}||CeO₂(111) and Pt{111}||CeO₂(111) interfaces with the
22 support, respectively (Fig. 1). The latter NP structure was found to be highly energetically
23 stable when supported on MgO(100) [54]. The Pt₉₅ NP was constructed from the energetically
24 stable MgO(100)-supported Pt₁₁₁ NP by removing 4 Pt atoms from each of the side {100}
25 nanofacets to decrease its lateral dimensions.

26 In the present touchstone study we explore in detail the alteration of structural and
27 electronic properties of Pt NPs by the CeO₂(111) support. We take full advantage of the
28 computational possibility to control the number of transferred electrons to characterize the
29 effects of Pt-ceria interaction depending on the amount of charge transfer. Briefly, we
30 obtained multiple configurations with the transfer of up to 6 electrons from Pt₉₅ and Pt₁₂₂
31 nanoparticles to CeO₂(111) support as detailed in the next section. The number of transferred
32 electrons was counted by the number of Ce⁴⁺ ions reduced to Ce³⁺ in each system. For the
33 sake of brevity, the the effect of charge transfer on properties of Pt-ceria system is discussed
34 only for configurations with the transfer of 0 and 6 electrons.



1

2 **Fig. 1.** Structure of the considered Pt_{95} and Pt_{122} nanoparticles forming $\text{Pt}_{95}\{100\}||\text{CeO}_2(111)$
 3 and $\text{Pt}_{122}\{111\}||\text{CeO}_2(111)$ interfaces, respectively, with the $\text{CeO}_2(111)$ support. (Edge) Pt
 4 atoms are (dark) blue, (surface) O atoms are (dark) red, Ce^{4+} cations are beige and Ce^{3+}
 5 cations – cyan. Dimensions of the employed $\text{CeO}_2(111)$ supercells are marked by black lines.

6 2. Computational details

7 VASP software [55] was used to perform spin-polarized calculations with the PW91
 8 exchange-correlation functional [56] augmented with Hubbard [57] $U = 4$ eV corrections on
 9 the f-states of all Ce atoms, adopted in line with previous studies [26,58]. Valence electrons
 10 were described using a plane-wave basis set with the cut-off energy of 415 eV, whereas core
 11 electrons were treated using projected augmented wave technique (PAW) [59]. The
 12 calculations were performed at the Γ -point in the reciprocal space and with 0.1 eV smearing
 13 applied to the electronic occupancies. All Pt atoms as well as atoms of the top O-Ce-O tri-
 14 layer of the $\text{CeO}_2(111)$ slabs were relaxed during geometry optimization until the forces
 15 acting on atoms decreased to 0.2 eV/nm. Atoms in the bottom tri-layer of two tri-layer thick
 16 $p(5\times 5)$ $\text{CeO}_2(111)$ slab with dimensions 1.909×1.909 nm² were fixed in the positions derived
 17 from the experimental bulk geometry. The sensitivity of the presented results to the chosen
 18 computational parameters has been examined elsewhere [23]. In particular, the number of
 19 transferred electrons was found to be essentially independent on the slab thickness and the
 20 choice of particular lattice parameter for the ceria surface, despite possible strain

1 accumulation in the support [60] and previous reports for Au atoms on CeO₂(111) [61]. The
2 separation between adjacent supported NPs was ~0.55 nm. At these distances there is an
3 attraction between each pair of adjacent Pt₉₅ and Pt₁₂₂ species with the strength calculated to
4 be 0.02 and 0.05 eV, respectively. Such weak interactions should not affect the conclusions of
5 the present study.

6 To obtain configurations with varying number of transferred electrons we took advantage
7 of the availability of pseudopotential for Ce³⁺ cations in VASP. In this case one occupied f-
8 state is introduced into the fixed pseudopotential core. Calculations where a part of Ce cations
9 had been represented by Ce³⁺ pseudopotentials were performed to pre-optimize geometries
10 with appropriately distorted ceria substrate for calculations employing only regular Ce
11 pseudopotentials. The discussion in this work is based only on results of the latter fully self-
12 consistent calculations yielding locally optimized geometries.

13 Namely, for each nanoparticle we started the calculations by forcing the reduction of all
14 25 surface Ce cations to Ce³⁺ through the use of Ce³⁺ pseudopotentials. For both supported
15 Pt₉₅ and Pt₁₂₂ nanoparticles such configurations were highly unstable and converged to
16 configurations with 6 electrons transferred from Pt to ceria when Ce³⁺ pseudopotentials were
17 substituted by regular Ce pseudopotentials without fixed f-electrons in the core. To obtain a
18 configuration with one less transferred electron we enforced the oxidation state of 4+ on the
19 Ce³⁺ cation with the lowest magnetization [62] in the previous configuration by setting its
20 magnetization to zero in the beginning of the calculation. By repeating this procedure we
21 obtained configurations with the transfer of zero to five electrons (Figure S1).

22 As a result, Ce³⁺ cations are located in similar positions for all obtained configurations of
23 the supported Pt₉₅ or Pt₁₂₂ particles. This way of calculation minimized oscillations of the
24 relative energies depending on the location of Ce³⁺ on the surface [60,62,63]. Note that in all
25 considered structures Ce³⁺ cations were located exclusively on the slab surface. Whereas on
26 pristine CeO₂(111) surfaces subsurface Ce³⁺ cations do not appear at low coverage $\theta(\text{Ce}^{3+}) <$
27 0.5 ML [64,65], more complex ceria-based systems may be more prone to develop subsurface
28 Ce³⁺ cations [62,66]. Another important remark is that the electron transfer from Pt particles
29 to the support was shown not to facilitate the formation of O vacancies in ceria [23].

30 **3. Results and discussion**

31 *3.1. Binding of Pt nanoparticles to CeO₂(111) support*

32 The strength of Pt-ceria interaction can be evaluated by the adhesion energy $E_{\text{adh}}[\text{Pt}_N]$
33 defined as $E_{\text{adh}}[\text{Pt}_N] = E[\text{supported Pt}_N/\text{ceria slab}] - E[\text{unsupported Pt}_N] - E[\text{ceria slab}]$, where

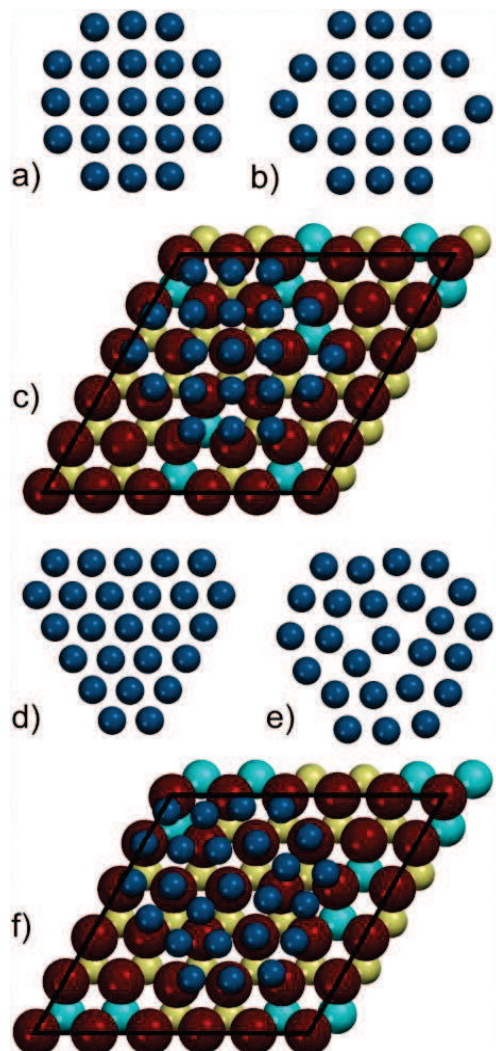
1 E[X] is the total energy of the system X. The adhesion energies of Pt₉₅ and Pt₁₂₂ NPs to
 2 CeO₂(111) in the most stable configurations regarding the electron transfer are calculated to
 3 be ~-15.0 eV and ~-9.6 eV, respectively. That is, the binding of Pt nanoparticles to CeO₂(111)
 4 through their {100} facets is notably stronger than through their {111} facets. This finding is
 5 in line with the lower coordination number of Pt atoms on Pt(100) terraces, N_{coord} = 8, than on
 6 Pt(111) terraces, N_{coord} = 9, and with concomitantly larger number of unsaturated bonds on the
 7 former surface. Indeed, the adhesion energy of Pt₉₅{100}||CeO₂(111) interface is -0.71 eV per
 8 each of 21 Pt atoms on the interface, that is, -8.97 eV/nm², whereas the strength of the
 9 interaction on Pt₁₂₂{111}||CeO₂(111) interface is -0.38 per each of 25 Pt atoms on the
 10 interface or -5.57 eV/nm². (Adhesion energies per nm² were calculated using the areas of the
 11 corresponding bottom facets of the unsupported Pt NPs.)

12 As a rule, the energetic stability of bare nanoparticles increases with the particle size
 13 [67,68], and so Pt₁₂₂ particles are more stable than Pt₉₅ species. One may circumvent this
 14 well-known dependency by considering the surface excess energy [54,69,70],
 15 $\Delta_{\text{exc}}[\text{unsupported Pt}_N] = N^{1/3} \times (E[\text{unsupported Pt}_N]/N - E[\text{Pt}_{\text{bulk}}])$ or $\Delta_{\text{exc}}[\text{supported Pt}_N/\text{ceria}]$
 16 $= N^{1/3} \times (\{E[\text{supported Pt}_N/\text{ceria}] - E[\text{ceria}]\}/N - E[\text{Pt}_{\text{bulk}}])$. According to this metric Pt₁₂₂ is
 17 still more stable than Pt₉₅ in the unsupported state with $\Delta_{\text{exc}}[\text{unsupported Pt}_{122}] = 3.44$ eV
 18 versus $\Delta_{\text{exc}}[\text{unsupported Pt}_{95}] = 3.78$ eV. The reason for the lower stability of the Pt₉₅ NP in
 19 the unsupported state is the presence of an extended bottom {100} facet, which has higher
 20 specific surface energy than {111} facets [71,72]. Nevertheless, surface excess energies of the
 21 two nanoparticles are equal in the supported state, $\Delta_{\text{exc}}[\text{supported Pt}_{95}/\text{ceria}] = \Delta_{\text{exc}}[\text{supported}$
 22 $\text{Pt}_{122}/\text{ceria}] = 3.05$ eV. Thus, the intrinsic lower stability of Pt₉₅ in the unsupported state is
 23 compensated by the stronger interaction between Pt₉₅{100} and the support. As a result, the
 24 two considered NPs forming either Pt{100}||CeO₂(111) or Pt{111}||CeO₂(111) interfaces
 25 appear to be equally energetically stable in the supported state according to our calculations.

26 3.2. Structure of the obtained Pt||CeO₂(111) interfaces

27 Pt nanoparticles were put on CeO₂(111) in a way that maximizes the number of Pt-O
 28 contacts (Fig. 2), which is typical for the contacts between extended Pt and ceria surfaces
 29 [41,50] and other Pt-oxide interfaces [53,54]. Note that only local structure optimization of
 30 the considered metal-oxide interfaces was performed in view of the computational
 31 inaccessibility of the global optimization. Although the bottom Pt₁₂₂{111} facet has a
 32 hexagonal symmetry like the symmetry of CeO₂(111) and the extended Pt₉₅{100} facet has a
 33 square symmetry, both facets undergo reconstruction upon contact with the ceria support. The

1 reconstruction is required for a better matching between Pt and O lattices, because of the
2 significant mismatch of the lattice parameters of the involved Pt and ceria surfaces. In the
3 calculated systems, the distance between O atoms on CeO₂(111) surface is 382 pm, whereas
4 the nearest Pt-Pt distances are ~280 pm.



5
6 **Fig. 2.** Bottom facets of a), d) unsupported and b), e) supported Pt₉₅ and Pt₁₂₂ nanoparticles,
7 respectively, as well as structures of c) Pt₉₅{100}||CeO₂(111) and f) Pt₁₂₂{111}||CeO₂(111)
8 interfaces. Color coding as in Fig. 1.

9 On the Pt₉₅{100}||CeO₂{111} interface two Pt atoms on the boundary displace outward
10 from the center of the interface in order to move from a “bridge” position between two
11 surface O closer to an “on top” position above surface O atoms. Curiously, this reconstruction
12 of the bottom facets is also locally stable in the unsupported Pt₉₅ NPs; however, it results in
13 1.25 eV higher energy than that of the unreconstructed unsupported Pt₉₅. The reconstruction
14 of the bottom {111} facet of supported Pt₁₂₂ NPs is more complex. The shape of the bottom Pt
15 facet changes from a hexagon with 2 and 5 atom long sides to a distorted hexagon with 3 and

1 4 atoms long sides and the interior area of the bottom facet adjusts accordingly. Such
2 reconstruction is locally unstable in unsupported Pt₁₂₂ NPs, which spontaneously relax to the
3 unreconstructed structure.

4 The calculated locations of Ce³⁺ ions formed upon the charge transfer seem to be
5 somewhat different for both types of the Pt-ceria interfaces. On the Pt₉₅{100}||CeO₂(111)
6 interface 4 out of 6 partially reduced Ce cations are located at the metal-oxide boundary,
7 whereas only one Ce³⁺ cation resides on the Pt₁₂₂{111}||CeO₂(111) interface. The other Ce³⁺
8 cations are located in the substrate areas that are not covered by Pt. Thus, we do not see an
9 obvious preference for Ce³⁺ cations to be located either under Pt NPs or away from them. A
10 dedicated rigorous study is required to identify possible more subtle inhomogeneities in the
11 distribution of Ce³⁺ cations. Note that the presence of Ce³⁺ cations on the ceria surface
12 uncovered by Pt may result in an interesting alteration of the substrate's reactivity.

13 *3.3. Effect of CeO₂(111) support on the geometric structure of Pt nanoparticles*

14 Previous computational studies have found the effect of CeO₂(111) support on the overall
15 geometric structure of small Pt clusters to be important [42,73]. However, in the case of
16 notably larger Pt₉₅ and Pt₁₂₂ nanoparticles only atomic positions in the bottom NP facets are
17 substantially affected by the support (Fig. 2). As a result there is an emergence of intermediate
18 Pt-Pt distances that may or may not be considered as interatomic bonds (Fig. S2). Note that
19 this was not the case for Pt NPs supported on MgO(100), where the strength of metal-oxide
20 interaction was not enough to cause the reconstruction of the nanoparticle facet [54]. For
21 example, supported Pt₉₅ particles exhibit Pt-Pt distances of ~370 pm, which are absent in
22 unsupported Pt₉₅ species. Similarly, Pt-Pt distances of ~340 pm in supported Pt₁₂₂ particles are
23 absent in the respective unsupported species. Thus, one cannot be certain if such Pt-Pt
24 distances are due to the formation of interatomic bonds between adjacent Pt atoms or due to
25 the coordination of Pt atoms by atoms in their second coordination sphere.

26 As a consequence, the average Pt-Pt bond-lengths in the supported nanoparticles can be
27 quantified in different ways (Table S1). On the one hand, one could consider only Pt-Pt
28 distances shorter than 340 pm (roughly the middle of the gap between the first and the second
29 coordination spheres in the unsupported Pt₁₂₂) as interatomic bonds. Then, the metal-support
30 interaction would result only in 0.3 and 0.6 pm average elongation of Pt-Pt bonds in Pt₉₅ and
31 Pt₁₂₂ particles, respectively. On the other hand, one could assume that the overall number of
32 Pt-Pt bonds in the nanoparticles does not change upon their interaction with CeO₂(111). Then,
33 the average Pt-Pt bonds would appear to be 4.6 and 5.8 pm longer in the supported Pt₉₅ and

1 Pt₁₂₂ nanoparticles than in the respective unsupported species, because in this case numerous
2 elongated Pt-Pt distances at the interface would be considered as bonds.

3 If the electron transfer from Pt nanoparticles to CeO₂(111) support is suppressed in the
4 calculations, then Pt-Pt bonds become even longer on average due to the higher resulting
5 occupancy of antibonding Pt-Pt d-states. In the case of supported Pt₉₅ particles the elongation
6 due to the suppressed electron donation to the support amounts to ~0.5 pm. At the same time,
7 the absence of the electron transfer leads to 0.2 or 1.3 pm longer Pt-Pt bonds in supported
8 Pt₁₂₂ nanoparticles depending on the method used to calculate the average bond distance.

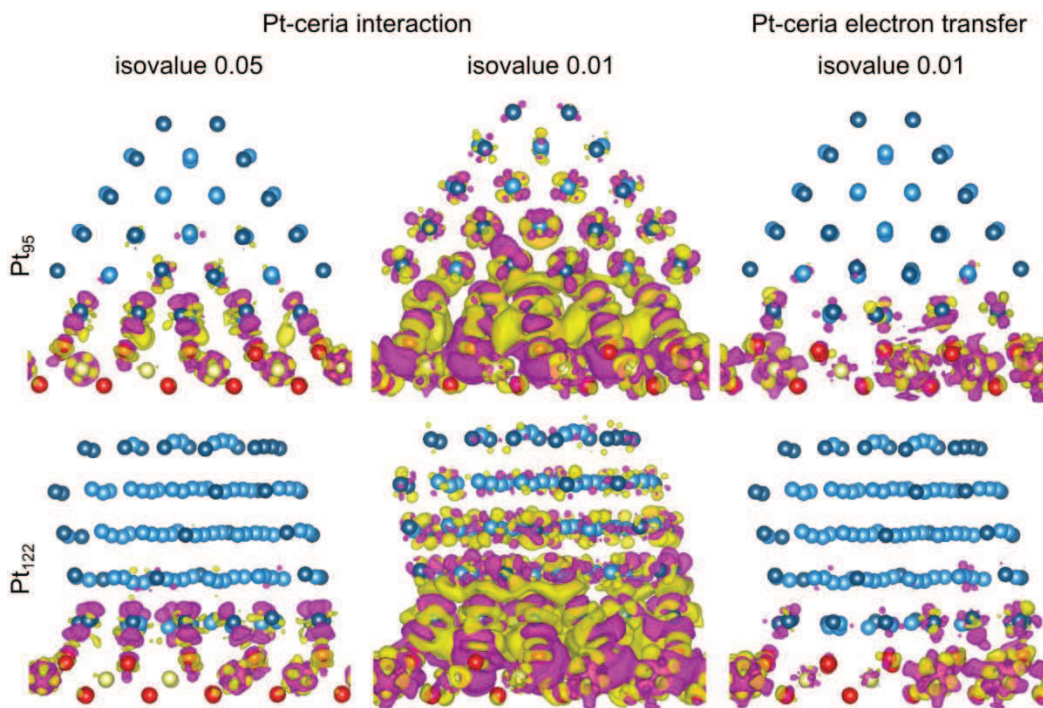
9 *3.4. Effect of CeO₂ on the electronic structure of supported Pt nanoparticles*

10 The contact between metallic Pt particles and ionic ceria support leads to the polarization
11 of the electron density of the former by near-surface electric fields, described previously for
12 the Pt(111)||CeO₂(111) interface [50]. The mutual polarization of Pt and ceria due to Pt-ceria
13 interaction can be visualized by means of charge density difference (CDD) plots, which
14 display isosurfaces of $\Delta\rho = \rho[\text{Pt}_N/\text{ceria}|_{6e}] - \rho[\text{Pt}_N] - \rho[\text{ceria}]$. In this formula $\rho[\text{Pt}_N]$ and
15 $\rho[\text{ceria}]$ are electron densities of individually calculated Pt NP and ceria support with
16 geometries from the optimized structure of supported Pt_N particle (with 6 transferred
17 electrons), which yields electron density $\rho[\text{Pt}_N/\text{ceria}|_{6e}]$. Isosurfaces plotted at isovalue of 0.05
18 atomic units (a. u.) show that the electron density in supported Pt nanoparticles moves from
19 the regions above negatively charged O anions towards regions above positively charged Ce
20 cations (Fig. 3). However, the polarization of electron density on Pt atoms diminishes rapidly
21 with growing distance to the ceria support (middle panels in Fig. 3). Note that the electron
22 density of Pt nanoparticles supported on CeO₂(111) is significantly more polarized than the
23 charge density of similar Pt nanoparticles on MgO(100) [54]. This can be explained by better
24 charge compensation within Tasker type I MgO(100) surface compared to Tasker type II
25 CeO₂(111) surface and by concomitantly stronger electric fields in the vicinity of the latter.

26 The electron density of the CeO₂(111) support also becomes polarized due to its
27 interaction with Pt. First, there is a visible change in the electron density of Ce cations that get
28 reduced from Ce⁴⁺ to Ce³⁺ upon Pt-ceria interaction. Second, one may notice a significant
29 polarization of the electron density on surface O anions that are in contact with Pt NP.

30 To focus on the contribution of the electron transfer to the polarization of the electron
31 density we generate CDD between two electronic states, with and without electron transfer:
32 $\Delta\rho_e = \rho[\text{Pt}_N/\text{ceria}|_{6e}] - \rho[\text{Pt}_N/\text{ceria}|_{0e}]$. Both states are calculated on the optimized geometry
33 with the transfer of 6 electrons. The resulting plots (right panels in Fig. 3) show that the

1 electron transfer leads to the polarization of reduced Ce^{3+} cations and Pt atoms on Pt-ceria
2 interface. Importantly, by comparing CDD for overall Pt-ceria interaction and solely for the
3 contribution of the electron transfer one concludes that the latter accounts for a mere fraction
4 of the polarization of electrons in Pt particles.

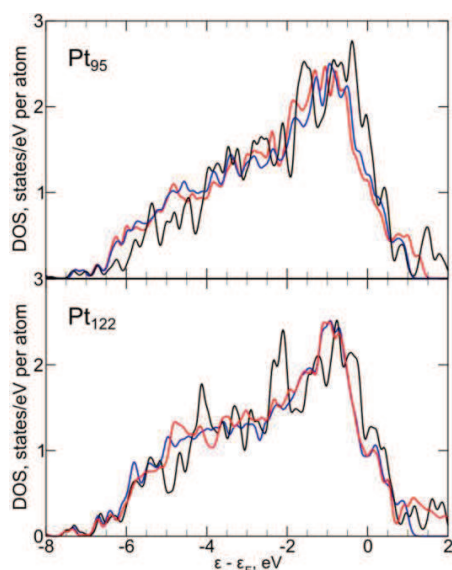


5
6 **Fig. 3.** Isosurfaces of charge density difference for the interaction between ceria and the
7 considered Pt particles involving the transfer of 6 electrons plotted at different isovalues (in
8 a.u.) as well as the distilled contribution of Pt-ceria electron transfer to the electron
9 polarization (see discussion). Regions of electron accumulation (depletion) are colored yellow
10 (pink). (Edge) Pt atoms are (dark) blue, O atoms are red, Ce cations are beige.

11 Bader charges provide another perspective on the polarization of electron density as a
12 result of Pt-ceria interactions (Table S2). The Bader charge on the nanoparticles in the
13 configurations without Ce^{3+} cations is 0.76 and 0.56 atomic units for Pt₉₅ and Pt₁₂₂,
14 respectively. However, the charge on nanoparticles increases only by ~ 1.3 a. u. when 6 Ce^{3+}
15 cations are present in the support. This finding is in agreement with the underestimation by
16 the Bader analysis of the difference between charges on Ce^{4+} , $\delta_{Bader}^+ = 2.4$, and Ce^{3+} , δ_{Bader}^+
17 $= 2.0$, cations. In line with the CDD analysis, Bader charges indicate that most of the charge
18 accumulated by the nanoparticle is located on the Pt atoms forming the interface with the
19 oxide support.

20 A similar conclusion can be drawn from the analysis of densities of states (DOS)
21 projected on atoms on the perimeter of the bottom facets of Pt nanoparticles, i.e. the facets

1 that form the interface with ceria. Indeed, there are some noticeable differences between the
 2 DOS projected on the bottom facets of the supported and unsupported nanoparticles (Fig. 4).
 3 The center of the occupied d-states projected on the bottom {111} facet of Pt₁₂₂ shifts down
 4 by 0.12 eV due to the interaction with CeO₂(111). The shift of the d-states is even more
 5 significant, 0.52 eV, for the bottom {100} facet of the Pt₉₅ NP, which interacts more strongly
 6 with CeO₂(111) than the Pt₁₂₂ species. Note that this shift is specific to CeO₂(111) support and
 7 not to all oxide supports. For example, MgO(100) support is calculated to have a negligible
 8 effect on the DOS of supported Pt particles [54].



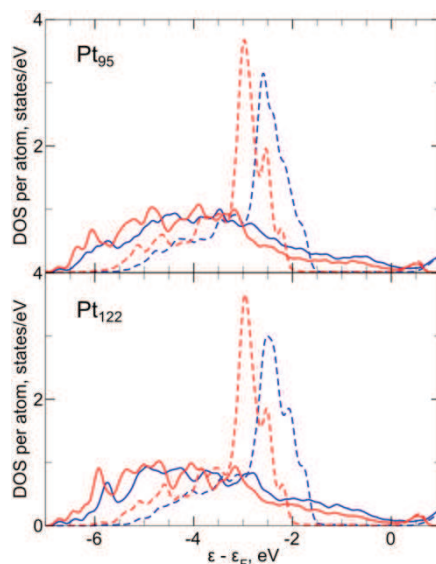
9
 10 **Fig. 4.** Electronic densities of states projected on Pt atoms on the metal-oxide boundary. Red
 11 line – the nanoparticles supported on CeO₂(111) in the absence of the electron transfer (no
 12 Ce³⁺); blue line – the nanoparticles on CeO₂(111) in the presence of the electron transfer (6
 13 Ce³⁺); black line – the respective atoms in unsupported nanoparticles. Electronic energies are
 14 given with respect to the Fermi level of each particular system.

15 At the same time, in line with results of CDD analysis, the electron transfer makes an
 16 insignificant contribution to the overall alteration of the electronic structure of Pt
 17 nanoparticles by the ceria support. The shifts of d-states due to the electron transfer were
 18 calculated to be less than 0.05 eV.

19 3.5. Effect of Pt nanoparticles on the electronic structure of CeO₂(111) support

20 Importantly, both the Pt-ceria interaction and the Pt-ceria electron transfer have a
 21 considerable effect on the electronic structure of surface O anions of the support. Fig. 5 shows
 22 that DOS projected on surface O in contact with Pt nanoparticles is qualitatively different
 23 from that of other O atoms on the same surface. Whereas DOS of the latter O atoms forms a

1 sharp peak between -3.5 and -1.5 eV with respect to the Fermi level, O atoms contacting with
 2 Pt exhibit a broad feature between -6.0 and -2.5 eV below the Fermi level in their DOS. The
 3 shift of O DOS to lower energies results in more significant overlap with Pt DOS extending
 4 up to -6.5 eV below the Fermi level, which strongly suggests the formation of the joint Pt-O
 5 electronic states.



6
 7 **Fig. 5.** Electronic densities of states projected on surface O atoms (solid line) on the metal-
 8 oxide boundary and (dashed line) not in contact with Pt. Red line – the nanoparticles
 9 supported on CeO₂(111) in the absence of the electron transfer (no Ce³⁺); blue line – the
 10 nanoparticles on CeO₂(111) in the presence of the electron transfer (6 Ce³⁺). Electronic
 11 energies are given with respect to the Fermi level.

12 In turn, the electron transfer affects DOS of surface O atoms, irrespective whether they
 13 form bonds with Pt or not. As a result of the transfer of 6 electrons from Pt nanoparticles to
 14 ceria support electronic states of O shift by 0.3-0.4 eV to higher energies. One can expect that
 15 the deposition-induced modifications of the electronic states of O anions at the Pt-ceria
 16 interface, including those related to the electron transfer from Pt to ceria, represent important
 17 channels for affecting the reactivity of Pt-ceria catalysts.

18 4. Conclusions

19 We investigated how interaction between Pt nanoparticles and defect-free CeO₂(111)
 20 support affects properties of the former using density-functional calculations. In particular, we
 21 considered 1.4 nm large Pt₉₅ and 1.5 nm large Pt₁₂₂ particles forming Pt{100}||CeO₂(111) and
 22 Pt{111}||CeO₂(111) interfaces. Both studied supported nanoparticles exhibit similar
 23 calculated energetic stability. This may be an indication of a similar thermodynamic stability

1 of both interfaces, implying that both interfaces could be observed experimentally. For both
2 nanoparticles we investigated how Pt-ceria interaction and transfer of 0 or 6 electrons to the
3 support affect the properties of the supported particles.

4 First, the metal-oxide interaction results in a certain elongation of average interatomic
5 distances in supported Pt nanoparticles. This elongation is accompanied by a reconstruction of
6 the Pt facet forming the interface with CeO₂(111) support due to the notable lattice mismatch
7 between Pt and ceria surfaces. Notably, the transfer of 6 electrons from Pt to ceria leads to the
8 contraction of Pt-Pt bonds by less than 1 pm on average. The Pt-ceria interaction also shifts
9 the electronic density of states of Pt atoms on the metal-oxide boundary to lower energies,
10 with the more significant shift for Pt atoms on Pt₉₅{100}||CeO₂(111) interface than on
11 Pt₁₂₂{111}||CeO₂(111). However, the role of the electron transfer in this shift appears to be
12 insignificant. Charge density difference analysis also indicates that Pt-ceria interaction leads
13 to a significant polarization of the electron density of Pt nanoparticles. However, again the
14 electron transfer does not affect the polarization as much as other components of the metal-
15 oxide interaction. At the same time, the electronic structure of O atoms on Pt-ceria interface is
16 profoundly affected by the metal-oxide interaction and the electron transfer. Moreover, some
17 Ce³⁺ cations are calculated to be present on the areas of ceria surface that were not covered by
18 Pt, which may alter the reactivity of the ceria substrate.

19 Note that the effects of Pt-ceria interaction on the geometric and the electronic structures
20 of the supported particles have been somewhat different for the two considered Pt₉₅ and Pt₁₂₂
21 species due to the different types of formed Pt-ceria interfaces. This finding suggests that the
22 effects of Pt-ceria interaction on the properties of Pt particles are also likely to depend on the
23 type of ceria surface forming the interface.

24 In summary, the electron transfer only modestly contributes to the overall ceria-induced
25 changes of the geometric and electronic structure of Pt particles that are large enough to be
26 relevant for technical catalysis (Pt₉₅ and Pt₁₂₂). In variation, sub-nanometer clusters such as
27 Pt₈ are shown to be strongly affected by the electron transfer to the ceria support [23]. Hence,
28 it is still uncertain at what particle size the metal-support electron transfer becomes important
29 for practical catalysis. The key requisite for a study addressing this problem is the ability to
30 control the magnitude of the metal-support electron transfer, which was achieved in the
31 present work for the important case of Pt-ceria model catalysts.

32 **Acknowledgments.** We gratefully acknowledge the support of the European Commission
33 (FP7-NMP.2012.1.1-1 project ChipCAT, Reference No. 310191), Spanish MINECO (grants

1 CTQ2012-34969 and CTQ2015-64618-R, co-funded by FEDER), as well as Generalitat de
2 Catalunya (grants 2014SGR97 and XRQTC). The research was also supported by Red
3 Española de Supercomputación.

4 **Appendix A**

5 Supplementary data associated with this article can be found in the online version.

6 **References**

- 7 [1] W. Yu, M.D. Porosoff, J.G. Chen, Review of Pt-based bimetallic catalysis: From model
8 surfaces to supported catalysts, *Chem. Rev.* 112 (2012) 5780–5817. doi:10.1021/cr300096b.
- 9 [2] G. Vilé, D. Albani, N. Almora-Barrios, N. López, J. Pérez-Ramírez, Advances in the Design of
10 Nanostructured Catalysts for Selective Hydrogenation, *ChemCatChem.* 8 (2016) 21–33.
11 doi:10.1002/cctc.201501269.
- 12 [3] T. Montini, M. Melchionna, M. Monai, P. Fornasiero, Fundamentals and Catalytic
13 Applications of CeO₂-Based Materials, *Chem. Rev.* 116 (2016) 5987–6041.
14 doi:10.1021/acs.chemrev.5b00603.
- 15 [4] K. Shimizu, Selective catalytic reduction of NO over supported silver catalysts-practical and
16 mechanistic aspects, *Phys. Chem. Chem. Phys.* 8 (2006) 2677–2695. doi:10.1039/b601794k.
- 17 [5] P. Azadi, R. Farnood, Review of heterogeneous catalysts for sub- and supercritical water
18 gasification of biomass and wastes, *Int. J. Hydrogen Energy.* 36 (2011) 9529–9541.
19 doi:10.1016/j.ijhydene.2011.05.081.
- 20 [6] B. Christian Enger, R. Lødeng, A. Holmen, A review of catalytic partial oxidation of methane
21 to synthesis gas with emphasis on reaction mechanisms over transition metal catalysts, *Appl.*
22 *Catal. A Gen.* 346 (2008) 1–27. doi:10.1016/j.apcata.2008.05.018.
- 23 [7] A. Ciftci, D.A.J.M. Ligthart, P. Pastorino, E.J.M. Hensen, Nanostructured ceria supported Pt
24 and Au catalysts for the reactions of ethanol and formic acid, *Appl. Catal. B Environ.* 130-131
25 (2013) 325–335. doi:10.1016/j.apcatb.2012.10.029.
- 26 [8] D.R. Rolison, Catalytic nanoarchitectures—the importance of nothing and the unimportance of
27 periodicity, *Science.* 299 (2003) 1698–701. doi:10.1126/science.1082332.
- 28 [9] S.M. Kozlov, K.M. Neyman, Insights from methane decomposition on nanostructured
29 palladium, *J. Catal.* 337 (2016) 111–121. doi:10.1016/j.jcat.2016.02.010.
- 30 [10] F. Calle-Vallejo, J. Tymoczko, V. Colic, Q.H. Vu, M.D. Pohl, K. Morgenstern, D. Loffreda, P.
31 Sautet, W. Schuhmann, A.S. Bandarenka, Finding optimal surface sites on heterogeneous
32 catalysts by counting nearest neighbors, *Science.* 350 (2015) 185–189.
33 doi:10.1126/science.aab3501.
- 34 [11] H.A. Aleksandrov, S.M. Kozlov, S. Schauermaun, G.N. Vayssilov, K.M. Neyman, How
35 absorbed hydrogen affects the catalytic activity of transition metals, *Angew. Chemie - Int. Ed.*
36 53 (2014) 13371–13375. doi:10.1002/anie.201405738.
- 37 [12] D. Teschner, J. Borsodi, A. Wootsch, Z. Révay, M. Hävecker, A. Knop-Gericke, S.D. Jackson,
38 R. Schlögl, The roles of subsurface carbon and hydrogen in palladium-catalyzed alkyne
39 hydrogenation, *Science.* 320 (2008) 86–89. doi:10.1126/science.1155200.
- 40 [13] A. Wolfbeisser, G. Kovács, S.M. Kozlov, K. Föttinger, J. Bernardi, B. Klötzer, K.M. Neyman,
41 G. Rupprechter, Surface composition changes of CuNi-ZrO₂ during methane decomposition:

- 1 An operando NAP-XPS and density functional study, *Catal. Today*. (2016).
2 doi:10.1016/j.cattod.2016.04.022.
- 3 [14] L. Cao, T. Mueller, Rational Design of Pt₃Ni Surface Structures for the Oxygen Reduction
4 Reaction, *J. Phys. Chem. C*. 119 (2015) 17735–17747. doi:10.1021/acs.jpcc.5b04951.
- 5 [15] M. Cargnello, J.J.D. Jaen, J.C.H. Garrido, K. Bakhmutsky, T. Montini, J.J.C. Gamez, R.J.
6 Gorte, P. Fornasiero, Exceptional Activity for Methane Combustion over Modular Pd@CeO₂
7 Subunits on Functionalized Al₂O₃, *Science*. 337 (2012) 713–717.
8 doi:10.1126/science.1222887.
- 9 [16] A. Bruix, Y. Lykhach, I. Matolínová, A. Neitzel, T. Skála, N. Tsud, M. Vorokhta, V.
10 Stetsovykh, K. Sevcikova, J. Mysliveček, R. Fiala, M. Václavů, K.C. Prince, S. Bruyère, V.
11 Potin, F. Illas, V. Matolín, J. Libuda, K.M. Neyman, Maximum noble-metal efficiency in
12 catalytic materials: Atomically dispersed surface platinum, *Angew. Chemie - Int. Ed.* 53 (2014)
13 10525–10530. doi:10.1002/anie.201402342.
- 14 [17] A. Bruix, J.A. Rodriguez, P.J. Ramirez, S.D. Senanayake, J. Evans, J.B. Park, D. Stacchiola, P.
15 Liu, J. Hrbek, F. Illas, A new type of strong metal-support interaction and the production of H₂
16 through the transformation of water on Pt/CeO₂(111) and Pt/CeO_x/TiO₂(110) catalysts, *J. Am.*
17 *Chem. Soc.* 134 (2012) 8968–8974. doi:10.1021/ja302070k.
- 18 [18] M. Cargnello, V.V.T. Doan-Nguyen, T.R. Gordon, R.E. Diaz, E.A. Stach, R.J. Gorte, P.
19 Fornasiero, C.B. Murray, Control of metal nanocrystal size reveals metal-support interface role
20 for ceria catalysts, *Science*. 341 (2013) 771–773. doi:10.1126/science.1240148.
- 21 [19] C.T. Campbell, Catalyst–support interactions: Electronic perturbations, *Nat. Chem.* 4 (2012)
22 597–598. doi:10.1038/nchem.1412.
- 23 [20] M. McEntee, A. Stevanovic, W. Tang, M. Neurock, J.T. Yates, Electric field changes on Au
24 nanoparticles on semiconductor supports - The molecular voltmeter and other methods to
25 observe adsorbate-induced charge-transfer effects in Au/TiO₂ Nanocatalysts, *J. Am. Chem.*
26 *Soc.* 137 (2015) 1972–1982. doi:10.1021/ja511982n.
- 27 [21] Y.P.G. Chua, G.T.K.K. Gunasooriya, M. Saeys, E.G. Seebauer, Controlling the CO oxidation
28 rate over Pt/TiO₂ catalysts by defect engineering of the TiO₂ support, *J. Catal.* 311 (2014) 306–
29 313. doi:10.1016/j.jcat.2013.12.007.
- 30 [22] D.R. Mullins, The surface chemistry of cerium oxide, *Surf. Sci. Rep.* 70 (2015) 42–85.
31 doi:10.1016/j.surfrep.2014.12.001.
- 32 [23] Y. Lykhach, S.M. Kozlov, T. Skála, A. Tovt, V. Stetsovykh, N. Tsud, F. Dvořák, V. Johánek,
33 A. Neitzel, J. Mysliveček, S. Fabris, V. Matolín, K.M.M. Neyman, J. Libuda, Counting
34 electrons on supported nanoparticles, *Nat. Mater.* 15 (2016) 284–289.
35 doi:10.1038/NMAT4500.
- 36 [24] J. Kugai, E.B. Fox, C. Song, Role of CeO₂ support for Pd-Cu bimetallic catalysts for oxygen-
37 enhanced water gas shift, *Appl. Catal. A Gen.* 456 (2013) 204–214.
38 doi:10.1016/j.apcata.2013.02.021.
- 39 [25] Y. Lykhach, V. Johánek, H.A. Aleksandrov, S.M. Kozlov, M. Happel, T. Skála, P.S. Petkov,
40 N. Tsud, G.N. Vayssilov, K.C. Prince, K.M. Neyman, V. Matolín, J. Libuda, Water chemistry
41 on model ceria and Pt/ceria catalysts, *J. Phys. Chem. C*. 116 (2012) 12103–12113.
42 doi:10.1021/jp302229x.
- 43 [26] A. Bruix, K.M. Neyman, Modeling Ceria-Based Nanomaterials for Catalysis and Related
44 Applications, *Catal. Letters*. (2016). doi:10.1007/s10562-016-1799-1.
- 45 [27] I.K. Naik, T.Y. Tien, Small-polaron mobility in nonstoichiometric cerium dioxide, *J. Phys.*

- 1 Chem. Solids. 39 (1978) 311–315. doi:10.1016/0022-3697(78)90059-8.
- 2 [28] J. Paier, C. Penschke, J. Sauer, Oxygen defects and surface chemistry of ceria: Quantum
3 chemical studies compared to experiment, Chem. Rev. 113 (2013) 3949–3985.
4 doi:10.1021/cr3004949.
- 5 [29] T. Duchoň, F. Dvořák, M. Aulická, V. Stetsovych, M. Vorokhta, D. Mazur, K. Veltruská, T.
6 Skála, J. Mysliveček, I. Matolínová, V. Matolín, Ordered phases of reduced ceria as epitaxial
7 films on Cu(111), J. Phys. Chem. C. 118 (2014) 357–365. doi:10.1021/jp409220p.
- 8 [30] M.A. Sk, S.M. Kozlov, K.H. Lim, A. Migani, K.M. Neyman, Oxygen vacancies in self-
9 assemblies of ceria nanoparticles, J. Mater. Chem. A. 2 (2014) 18329–18338.
10 doi:10.1039/C4TA02200A.
- 11 [31] V. Matolín, I. Matolínová, L. Sedláček, K.C. Prince, T. Skála, A resonant photoemission
12 applied to cerium oxide based nanocrystals, Nanotechnology. 20 (2009) 215706.
13 doi:10.1088/0957-4484/20/21/215706.
- 14 [32] U. Berner, K. Schierbaum, G. Jones, P. Wincott, S. Haq, G. Thornton, Ultrathin ordered CeO₂
15 overlayers on Pt(111): Interaction with NO₂, NO, H₂O and CO, Surf. Sci. 467 (2000) 201–213.
16 doi:10.1016/S0039-6028(00)00770-6.
- 17 [33] K. Ševcikova, V. Nehasil, M. Vorokhta, S. Haviar, V. Matolín, I. Matolínová, K. Mašek, I. Piš,
18 K. Kobayashi, M. Kobata, T. Nagata, Y. Matsushita, H. Yoshikawa, Altering properties of
19 cerium oxide thin films by Rh doping, Mater. Res. Bull. 67 (2015) 5–13.
20 doi:10.1016/j.materresbull.2015.02.059.
- 21 [34] G.N. Vayssilov, Y. Lykhach, A. Migani, T. Staudt, G.P. Petrova, N. Tsud, T. Skála, A. Bruix,
22 F. Illas, K.C. Prince, V. Matolín, K.M. Neyman, J. Libuda, Support nanostructure boosts
23 oxygen transfer to catalytically active platinum nanoparticles, Nat. Mater. 10 (2011) 310–315.
24 doi:10.1038/nmat2976.
- 25 [35] G. Lafaye, J. Barbier, D. Duprez, Impact of cerium-based support oxides in catalytic wet air
26 oxidation: Conflicting role of redox and acid-base properties, Catal. Today. 253 (2015) 89–98.
27 doi:10.1016/j.cattod.2015.01.037.
- 28 [36] A. Alijani, A. Irankhah, Medium-Temperature Shift Catalysts for Hydrogen Purification in a
29 Single-Stage Reactor, Chem. Eng. Technol. 36 (2013) 209–219. doi:10.1002/ceat.201200151.
- 30 [37] O. Pozdnyakova, D. Teschner, A. Wootsch, J. Kröhnert, B. Steinhauer, H. Sauer, L. Toth, F.C.
31 Jentoft, A. Knop-Gericke, Z. Paál, R. Schlögl, Preferential CO oxidation in hydrogen (PROX)
32 on ceria-supported catalysts, part I: Oxidation state and surface species on Pt/CeO₂ under
33 reaction conditions, J. Catal. 237 (2006) 1–16. doi:10.1016/j.jcat.2005.10.014.
- 34 [38] T. Zheng, J. He, Y. Zhao, W. Xia, J. He, Precious metal-support interaction in automotive
35 exhaust catalysts, J. Rare Earths. 32 (2014) 97–107. doi:10.1016/S1002-0721(14)60038-7.
- 36 [39] P. Ciambelli, V. Palma, A. Ruggiero, Low temperature catalytic steam reforming of ethanol. 1.
37 The effect of the support on the activity and stability of Pt catalysts, Appl. Catal. B Environ. 96
38 (2010) 18–27. doi:10.1016/j.apcatb.2010.01.029.
- 39 [40] M. Happel, J. Mysliveček, V. Johánek, F. Dvořák, O. Stetsovych, Y. Lykhach, V. Matolín, J.
40 Libuda, Adsorption sites, metal-support interactions, and oxygen spillover identified by
41 vibrational spectroscopy of adsorbed CO: A model study on Pt/ceria catalysts, J. Catal. 289
42 (2012) 118–126. doi:10.1016/j.jcat.2012.01.022.
- 43 [41] P. Luches, L. Giordano, V. Grillo, G.C. Gazzadi, S. Prada, M. Campanini, G. Bertoni, C.
44 Magen, F. Pagliuca, G. Pacchioni, S. Valeri, Atomic Scale Structure and Reduction of Cerium
45 Oxide at the Interface with Platinum, Adv. Mater. Interfaces. 2 (2015) 1500375.

- 1 doi:10.1002/admi.201500375.
- 2 [42] F.R. Negreiros, S. Fabris, Role of Cluster Morphology in the Dynamics and Reactivity of
3 Subnanometer Pt Clusters Supported on Ceria Surfaces, *J. Phys. Chem. C*. 118 (2014) 21014–
4 21020. doi:10.1021/jp506404z.
- 5 [43] S. Nishimura, K. Ebitani, Recent Advances in Heterogeneous Catalysis with Controlled
6 Nanostructured Precious Monometals, *ChemCatChem*. 8 (2016) 2303–2316.
7 doi:10.1002/cctc.201600309.
- 8 [44] A.S. Crampton, M.D. Rötzer, F.F. Schweinberger, B. Yoon, U. Landman, U. Heiz, Ethylene
9 hydrogenation on supported Ni, Pd and Pt nanoparticles: Catalyst activity, deactivation and the
10 d-band model, *J. Catal.* 333 (2016) 51–58. doi:10.1016/j.jcat.2015.10.023.
- 11 [45] S.M. Kozlov, K.M. Neyman, Catalysis from first principles: Towards accounting for the effects
12 of nanostructuring, *Top. Catal.* 56 (2013) 867–873. doi:10.1007/s11244-013-0050-1.
- 13 [46] I. V. Yudanov, A. Genest, S. Schauermaun, H.J. Freund, N. Rösch, Size Dependence of the
14 adsorption energy of CO on metal nanoparticles: A DFT search for the minimum value, *Nano*
15 *Lett.* 12 (2012) 2134–2139. doi:10.1021/nl300515z.
- 16 [47] Y. Zhou, J.M. Perket, J. Zhou, Growth of Pt nanoparticles on reducible CeO₂(111) thin films:
17 Effect of nanostructures and redox properties of Ceria, *J. Phys. Chem. C*. 114 (2010) 11853–
18 11860. doi:10.1021/jp1007279.
- 19 [48] K.-D. Schierbaum, Ordered ultra-thin cerium oxide overlayers on Pt(111) single crystal
20 surfaces studied by LEED and XPS, *Surf. Sci.* 399 (1998) 29–38. doi:10.1016/S0039-
21 6028(97)00808-X.
- 22 [49] P. Luches, S. Valeri, Structure, morphology and reducibility of epitaxial cerium oxide ultrathin
23 films and nanostructures, *Materials*. 8 (2015) 5818–5833. doi:10.3390/ma8095278.
- 24 [50] C. Spiel, P. Blaha, Y. Suchorski, K. Schwarz, G. Rupprechter, CeO₂/Pt(111) interface studied
25 using first-principles density functional theory calculations, *Phys. Rev. B*. 84 (2011) 045412.
26 doi:10.1103/PhysRevB.84.045412.
- 27 [51] D. Loffreda, F. Delbecq, Growth of a Pt film on non-reduced ceria: A density functional theory
28 study, *J. Chem. Phys.* 136 (2012) 044705. doi:10.1063/1.3678864.
- 29 [52] C. Gatel, P. Baules, E. Snoeck, Morphology of Pt islands grown on MgO(001), *J. Cryst.*
30 *Growth*. 252 (2003) 424–432. doi:10.1016/S0022-0248(03)00868-6.
- 31 [53] J. Olander, R. Lazzari, J. Jupille, B. Mangili, J. Goniakowski, G. Renaud, Size- and
32 temperature-dependent epitaxy for a strong film-substrate mismatch: The case of Pt/MgO(001),
33 *Phys. Rev. B*. 76 (2007) 075409. doi:10.1103/PhysRevB.76.075409.
- 34 [54] S.M. Kozlov, H.A. Aleksandrov, J. Goniakowski, K.M. Neyman, Effect of MgO(100) support
35 on structure and properties of Pd and Pt nanoparticles with 49-155 atoms, *J. Chem. Phys.* 139
36 (2013) 084701. doi:10.1063/1.4817948.
- 37 [55] G. Kresse, J. Furthmüller, Efficient iterative schemes for ab initio total-energy calculations
38 using a plane-wave basis set, *Phys. Rev. B*. 54 (1996) 11169–11186.
39 doi:10.1103/PhysRevB.54.11169.
- 40 [56] J.P. Perdew, Y. Wang, Accurate and simple analytic representation of the electron-gas
41 correlation energy, *Phys. Rev. B*. 45 (1992) 13244–13249.
- 42 [57] S.L. Dudarev, G.A. Botton, S.Y. Savrasov, C.J. Humphreys, A.P. Sutton, Electron-energy-loss
43 spectra and the structural stability of nickel oxide: An LSDA+U study, *Phys. Rev. B*. 57 (1998)

- 1 1505–1509.
- 2 [58] C. Loschen, J. Carrasco, K.M. Neyman, F. Illas, First-principles LDA+U and GGA+U study of
3 cerium oxides: Dependence on the effective U parameter, *Phys. Rev. B.* 75 (2007) 035115.
4 doi:10.1103/PhysRevB.75.035115.
- 5 [59] G. Kresse, D. Joubert, From ultrasoft pseudopotentials to the projector augmented-wave
6 method, *Phys. Rev. B.* 59 (1999) 1758–1775. doi:10.1103/PhysRevB.59.1758.
- 7 [60] M.V. Ganduglia-Pirovano, J.L.F. Da Silva, J. Sauer, Density-functional calculations of the
8 structure of near-surface oxygen vacancies and electron localization on CeO₂(111), *Phys. Rev.*
9 *Lett.* 102 (2009) 026101. doi:10.1103/PhysRevLett.102.026101.
- 10 [61] M.M. Branda, N.J. Castellani, R. Grau-Crespo, N.H. De Leeuw, N.C. Hernandez, J.F. Sanz,
11 K.M. Neyman, F. Illas, On the difficulties of present theoretical models to predict the oxidation
12 state of atomic Au adsorbed on regular sites of CeO₂(111), *J. Chem. Phys.* 131 (2009) 094702.
13 doi:10.1063/1.3216102.
- 14 [62] S.M. Kozlov, K.M. Neyman, O vacancies on steps on the CeO₂(111) surface, *Phys. Chem.*
15 *Chem. Phys.* 16 (2014) 7823–7829. doi:10.1039/c4cp00136b.
- 16 [63] A. Migani, K.M. Neyman, F. Illas, S.T. Bromley, Exploring Ce³⁺/Ce⁴⁺ cation ordering in
17 reduced ceria nanoparticles using interionic-potential and density-functional calculations, *J.*
18 *Chem. Phys.* 131 (2009) 064701. doi:10.1063/1.3195063.
- 19 [64] Y.-G. Wang, D. Mei, J. Li, R. Rousseau, DFT+U Study on the Localized Electronic States and
20 Their Potential Role During H₂O Dissociation and CO Oxidation Processes on CeO₂(111)
21 Surface, *J. Phys. Chem. C.* 117 (2013) 23082–23089. doi:10.1021/jp409953u.
- 22 [65] G.E. Murgida, M.V. Ganduglia-Pirovano, Evidence for subsurface ordering of oxygen
23 vacancies on the reduced CeO₂(111) surface using density-functional and statistical
24 calculations, *Phys. Rev. Lett.* 110 (2013) 246101. doi:10.1103/PhysRevLett.110.246101.
- 25 [66] K. Košmider, V. Brázdová, M.V. Ganduglia-Pirovano, R. Pérez, Do Au Atoms Titrate Ce³⁺
26 Ions at the CeO_{2-x}(111) Surface?, *J. Phys. Chem. C.* 120 (2016) 927–933.
27 doi:10.1021/acs.jpcc.5b05335.
- 28 [67] A. Roldán, F. Viñes, F. Illas, J.M. Ricart, K.M. Neyman, Density functional studies of coinage
29 metal nanoparticles: Scalability of their properties to bulk, *Theor. Chem. Acc.* 120 (2008) 565–
30 573. doi:10.1007/s00214-008-0423-x.
- 31 [68] I. V. Yudanov, A. Genest, N. Rösch, DFT Studies of Palladium Model Catalysts: Structure and
32 Size Effects, *J. Clust. Sci.* 22 (2011) 433–448. doi:10.1007/s10876-011-0392-4.
- 33 [69] T. Halicioglu, Properties of Diamond and Diamond-like Clusters in Nanometric Dimensions,
34 *Phys. Status Solidi.* 199 (1997) 345–350.
- 35 [70] W. Vervisch, C. Mottet, J. Goniakowski, Theoretical study of the atomic structure of Pd
36 nanoclusters deposited on a MgO(100) surface, *Phys. Rev. B.* 65 (2002) 245411.
37 doi:10.1103/PhysRevB.65.245411.
- 38 [71] S.H. Yoo, J.H. Lee, Y.K. Jung, A. Soon, Exploring stereographic surface energy maps of cubic
39 metals via an effective pair-potential approach, *Phys. Rev. B.* 93 (2016) 035434.
40 doi:10.1103/PhysRevB.93.035434.
- 41 [72] L. Vitos, A. V. Ruban, H.L. Skriver, J. Kollár, The surface energy of metals, *Surf. Sci.* 411
42 (1998) 186–202. doi:10.1016/S0039-6028(98)00363-X.
- 43 [73] A. Bruix, A. Migani, G.N. Vayssilov, K.M. Neyman, J. Libuda, F. Illas, Effects of deposited Pt

1 particles on the reducibility of CeO₂(111), Phys. Chem. Chem. Phys. 13 (2011) 11384–11392.
2 doi:10.1039/c1cp20950g.